



# Modelling Stress-Strain Behaviour of Low-Yield-Point Steels

Fangxin Hu<sup>1,2</sup> 

<sup>1</sup> School of Civil Engineering and Transportation, South China University of Technology, Guangzhou 510640, China

hufx@scut.edu.cn

<sup>2</sup> State Key Laboratory of Subtropical Building Science, South China University of Technology, Guangzhou 510640, China

**Abstract.** Unlike low carbon or alloy steels, low-yield-point steels are characterized with very low yield strength but very high capacity of strain hardening and deformation capacity. In order to develop their advantages in energy dissipation systems, accurate modeling of the stress-strain behavior of low-yield-point steels are imperative for structural analysis and performance evaluation. Previous experimental investigations have revealed the prominent cyclic hardening response and there generally exists an initial yield plateau. Based on these observations, a cyclic plasticity model was developed to describe the stress-strain responses under monotonic and various cyclic loadings. Both isotropic hardening and kinematic hardening were found to be nonlinear. Exponential function was used to describe the transient hardening under cyclic loading, while evolution of backstresses based on the Armstrong-Frederick rule was used to trace the significant Bauschinger effect in unloading-reloading cycles. Both isotropic and kinematic hardening rules were decomposed into short-range and long-range components to capture the stress-strain responses in yield plateau and strain-hardening regions, respectively, but using formulations of different parameters. In addition, an impermanent bounding surface in stress space and a memory surface in plastic strain space were established to correctly describe the yield plateau stress and duration. A calibration procedure by tension coupon test was established, which makes it convenient to determine model parameters in practical application. Close agreement between the experimental and the modeling stress-strain curves was obtained. Therefore, the developed cyclic plasticity model can be used for further elasto-plastic analysis of structural components or systems using low-yield-point steels to yield accurate predictions.

**Keywords:** Low-yield-point steel · Stress-strain model · Cyclic plasticity

Low-yield-point steels are widely applied in energy dissipation members. Their cyclic behaviour under earthquake loadings has significant influence on the structural performance. Therefore, it is necessary to develop cyclic plasticity model of such steels for accurate evaluation of their energy dissipation capacities. Nowadays, there have been lots of experimental studies on cyclic responses of low-yield-point steels [1–6], but how to model their stress-strain responses accurately still remains a practical problem. This paper is mainly devoted to the verification of a cyclic plasticity model developed by the author for mild steels [7, 8] in prediction of stress-strain relations of low-yield-point

steels with nominal yield strength lower than 235 MPa, which are much different from conventional mild steels in that they generally have much lower yield-to-tensile strength ratios and thus, more significant strain hardening beyond yield plateau.

## 1 Review of Cyclic Plasticity Model [7, 8]

### 1.1 General Equations

The total strain rate tensor is decomposed into elastic and plastic strain rate components as

$$\dot{\boldsymbol{\varepsilon}} = \dot{\boldsymbol{\varepsilon}}^e + \dot{\boldsymbol{\varepsilon}}^p \quad (1)$$

where the elastic strain rate is associated with the stress rate by Hooke's law. The plastic behaviour is characterized by von Mises yield surface

$$f = \bar{\sigma} - R = \sqrt{\frac{3}{2}(\boldsymbol{s} - \boldsymbol{\alpha}) : (\boldsymbol{s} - \boldsymbol{\alpha})} - R = 0 \quad (2)$$

where  $\bar{\sigma}$  is the effective von Mises stress and  $R$  is the radius of yield surface;  $\boldsymbol{\alpha}$  is the back stress tensor and  $\boldsymbol{s}$  is deviatoric stress tensor which is defined as

$$\boldsymbol{s} = \boldsymbol{\sigma} - \frac{1}{3}\text{tr}(\boldsymbol{\sigma})\mathbf{1} \quad (3)$$

where "tr" indicates the trace operator and  $\boldsymbol{\sigma}$  is the stress tensor. Associated flow rule is used to determine the plastic strain rate tensor as

$$\dot{\boldsymbol{\varepsilon}}^p = \dot{\lambda} \frac{\partial f}{\partial \boldsymbol{\sigma}} = \frac{3}{2} \boldsymbol{n} \dot{\boldsymbol{\varepsilon}}^p = \frac{3}{2} \frac{\boldsymbol{s} - \boldsymbol{\alpha}}{\bar{\sigma}} \dot{\boldsymbol{\varepsilon}}^p \quad (4)$$

where  $\boldsymbol{n}$  is the flow direction normal to the yield surface, and  $\dot{\bar{\boldsymbol{\varepsilon}}}^p$  denotes the equivalent plastic strain rate, which is defined as

$$\dot{\bar{\boldsymbol{\varepsilon}}}^p = \sqrt{\frac{2}{3} \dot{\boldsymbol{\varepsilon}}^p : \dot{\boldsymbol{\varepsilon}}^p} \quad (5)$$

### 1.2 Hardening Rules

Classical nonlinear isotropic and kinematic hardening rules are used. Isotropic hardening is described by

$$\dot{R} = \sum_j \dot{R}_j \quad (6)$$

$$\dot{R}_j = b_j (Q_j - R_j) \dot{\bar{\boldsymbol{\varepsilon}}}^p \quad (7)$$

where  $\dot{R}$  is the total change rate of the radius of yield surface and it is decomposed into multiple components  $\dot{R}_j$  each with independent hardening parameters  $b_j$  and  $Q_j$ . Note that  $Q_j$  represents the saturated value of  $R_j$  and a positive value of that indicates isotropic hardening, and softening otherwise, while  $b_j$  represents the rate of evolution.

Kinematic hardening is described by the evolution law proposed by Armstrong and Frederick [9] in the form

$$\dot{\alpha} = \sum_j \dot{\alpha}_j \quad (8)$$

$$\dot{\alpha}_j = \frac{2}{3} C_j \dot{\epsilon}^p - \gamma_j \alpha_j \dot{\epsilon}^p \quad (9)$$

where  $\dot{\alpha}$  is the total backstress rate and it is also decomposed into multiple tensor components  $\dot{\alpha}_j$  each with independent hardening parameters  $C_j$  and  $\gamma_j$ .

A memory surface is defined in plastic strain space as

$$g = \sqrt{\frac{2}{3} (\epsilon^p - \xi) : (\epsilon^p - \xi)} - r = 0 \quad (10)$$

where

$$\dot{\xi} = (1 - c)H(g) \left\langle \mathbf{m} : \frac{2}{3} \dot{\epsilon}^p \right\rangle \mathbf{m} \quad (11)$$

$$\dot{r} = cH(g) \langle \mathbf{n} : \mathbf{m} \rangle \dot{\epsilon}^p \quad (12)$$

where  $r$  is the radius of the memory surface;  $c$  is a scalar material parameter which determines the rate of expansion of the memory surface;  $H(g)$  is Heaviside function, i.e.  $H(g) = 1$  if  $g = 0$  and  $H(g) = 0$  if  $g < 0$ ;  $\langle \rangle$  denotes the Macaulay brackets, i.e.  $\langle a \rangle = a$  if  $a > 0$  and  $\langle a \rangle = 0$  if  $a < 0$ ;  $\mathbf{m}$  is the direction normal to the memory surface:

$$\mathbf{m} = \frac{\epsilon^p - \xi}{r} \quad (13)$$

Isotropic softening or hardening is deactivated when the plastic strain state lies inside the memory surface. Thus, two sets of parameters  $c^s$  and  $c^l$  are used for short-range and long-range hardening, respectively.

Another important parameter  $\bar{\epsilon}_{st}^p$  is also included to determine whether current stress state belong to the plateau region or hardening region. The following criterion proposed by Ucak and Tsopelas [10] is assumed

$$\begin{aligned} & \text{if } r \leq \bar{\epsilon}_{st}^p \text{ or } \bar{\epsilon}^p \leq \bar{\epsilon}_{st}^p \rightarrow \text{plateau region} \\ & \text{if } r > \bar{\epsilon}_{st}^p \text{ and } \bar{\epsilon}^p > \bar{\epsilon}_{st}^p \rightarrow \text{hardening region} \end{aligned} \quad (14)$$

### 1.3 Parameter Calibration

A concise calibration procedure for isotropic and kinematic hardening parameters by monotonic true stress-plastic strain curve is established. The engineering stress ( $s$ )-strain ( $e$ ) relation should be transformed into a true relation by

$$\varepsilon = \ln(1 + e) \quad (15)$$

$$\sigma = (1 + e)s \quad (16)$$

Then elastic modulus  $E$  and yield stress  $\sigma_y$  can be directly determined. Since necking initiates at peak load, the true stress and plastic strain can be computed from nominal ones by a weighted average method by Jia and Kuwamura [11], by assuming that the true stress is linearly correlated with the true strain after the ultimate true stress  $\sigma_u$ . The linear hardening modulus with respect to the plastic strain is

$$H = w\sigma_u / \left(1 - \frac{w\sigma_u}{E}\right) \quad (17)$$

where  $w$  is a factor calibrated based on the descending part of nominal stress-strain curve.

The derived monotonic true stress-plastic strain curve by the above procedure represents the upper bound of elastic range. However, the lower bound of elastic range is generally unknown. Thus, a critical assumption is made that the reversal yield stress under moderate strain amplitudes is the same, which means the yield surface saturates after initial contraction in size, as shown in Fig. 1. When the plastic strain exceeds  $\varepsilon_u^p$ , the lower bound is parallel to the upper true stress-plastic strain bound, which means the yield surface saturates after subsequent expansion in size and translates only. Based on such an assumption, the initial contraction of the yield surface is described by using a short-range isotropic softening component, whose saturation  $Q^s (< 0)$  and rate parameter  $b^s$  should be calibrated by the cyclic stress-strain relations.

To ensure the consistency of positive hardening modulus, two short-range non-linear backstress components  $\alpha_1^s$  and  $\alpha_2^s$  evolve along with the above isotropic softening component with equivalent saturation and some other empirical relations

$$-Q^s = \sum_{j=1}^2 \frac{C_j^s}{\gamma_j^s} \quad \text{and} \quad \frac{C_1^s}{\gamma_1^s} : \frac{C_2^s}{\gamma_2^s} = 1 : 2 \quad \text{and} \quad \gamma_1^s = 10\gamma_2^s \quad \text{and} \quad \gamma_2^s = b^s \quad (18)$$

The linear hardening modulus at final stage makes it natural to build a long-range linear backstress component  $\alpha_2^l$  with hardening parameters

$$C_2^l = H \quad \text{and} \quad \gamma_2^l = 0 \quad (19)$$

Thus, the rest hardening components, including a long-range backstress  $\alpha_1^l$  and an isotropic hardening component, can be derived by the geometric relations in Fig. 1. Their parameters satisfy

$$\frac{C_1^l}{\gamma_1^l} = \frac{\sigma_u - \sigma_y}{2} - H(\varepsilon_u^p - \varepsilon_{st}^p) \quad (20)$$

$$Q^l = \frac{\sigma_u - \sigma_y}{2} \quad (21)$$

The rate parameters  $\gamma_1^l$  and  $b^l$  are then calibrated to fit the monotonic stress-strain curve shape.

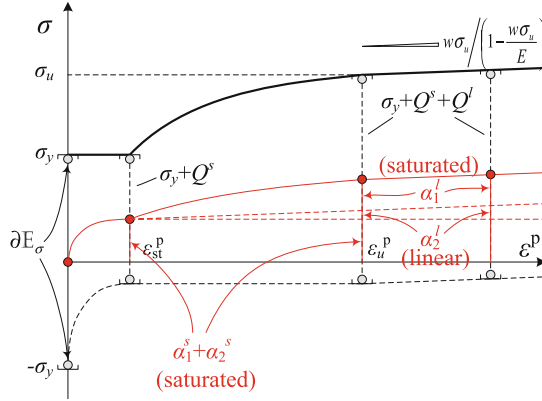


Fig. 1. Decomposition of hardening components.

## 2 Comparison with Experimental Results

In order to calibrate and validate the cyclic plasticity model for low-yield-point steels, a systematic experimental investigation by Shi et al. [5] is referred to. In their study, coupon specimens made of LY100, LY160 and LY225 low-yield-point steels produced in China were subjected to monotonic tension and 12 different cyclic loadings, including various constant-amplitude, variable increasing- and decreasing-amplitude as well as some random histories. Based on the stress-strain database obtained by Shi et al. [5] and using the calibration method illustrated above, the material parameters of those LY100, LY160 and LY225 steels were determined as shown in Table 1. Comparison between experimental and modelling results are then shown in Fig. 2 for LY160 steel under 6 representative cyclic loadings, and in Fig. 3 and Fig. 4 for LY100 and LY225 steels, respectively, under a representative increasing-amplitude and a representative constant-amplitude cyclic loading. Not all the results of 12 cyclic loadings are presented to save space. It is clear that the sudden initial yield drop phenomenon is not considered and thus not captured in the modelling, but the plateau response following that is simulated well. The stress amplitudes are well captured, but the cyclic stress evolution is underestimated at relatively large-amplitude cycles. Generally, close agreement is obtained and the accuracy of the cyclic plasticity model in terms of application in steel structural engineering is evidenced.

**Table 1.** Calibrated parameters.

Steel Gr.	$E$ $\sigma_y$	$\epsilon_{st}^p$ $\epsilon_{st}^d$	$Q^s$ $b^s$	$Q^l$ $b^l$	$C_1^s$ $\gamma_1^s$	$C_2^s$ $\gamma_2^s$	$C_1^l$ $\gamma_1^l$	$C_2^l$ $\gamma_2^l$	$c^s$ $c^l$
LY100	199000	0.0134	-43.8	94.8	116881.3	23376.3	2223.8	235.3	0.5
	133.1	0.005	800	40	8000	800	50	0	0.1
LY160	194000	0.0099	-54.7	94.3	145784.8	29157	2301.1	260	0.5
	182.2	0.005	800	20	8000	800	50	0	0.1
LY225	202500	0.0238	-95.6	86.7	191177.6	57353.3	1565	255.6	0.4
	191.2	0.005	800	16	8000	800	40	0	0.3

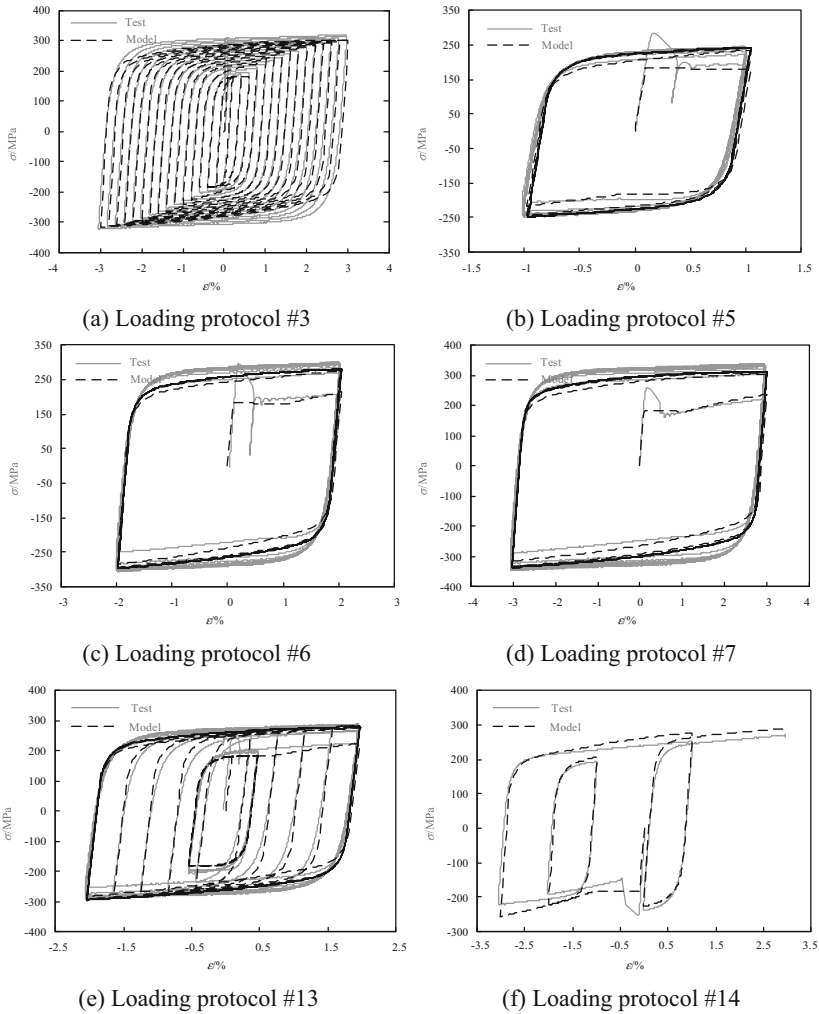


**Fig. 2.** Stress-strain responses of LY160 steel.

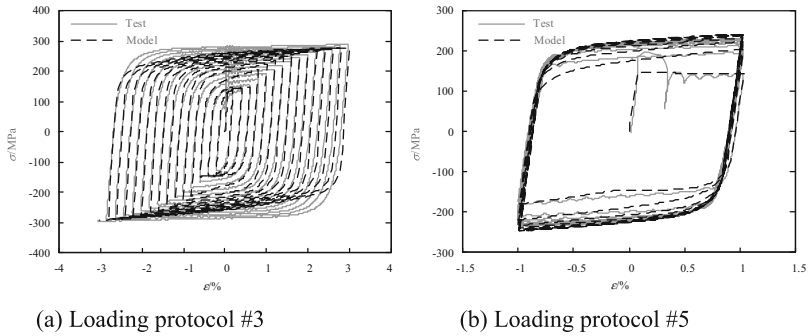


**Fig. 3.** Stress-strain responses of LY100 steel.

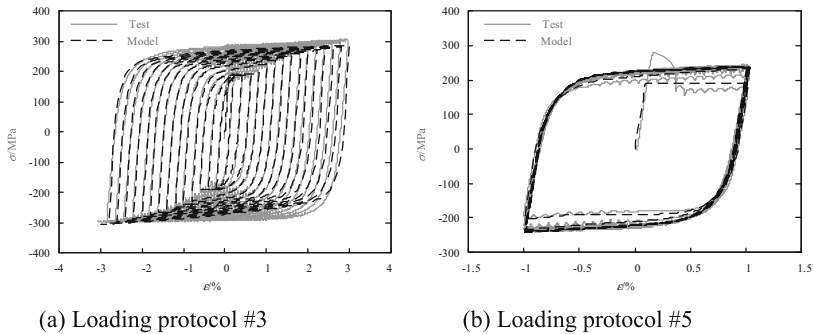


**Fig. 4.** Stress-strain responses of LY225 steel.

### 3 Conclusions

Cyclic plasticity models developed previously by the author for mild steels is used to model stress-strain responses of low-yield-point steels under monotonic and various cyclic loadings. The cyclic plasticity model is validated against the experimental responses and can be used further for seismic or dynamic analysis of steel structures using those steels.

The author has developed Abaqus UMAT subroutines for the cyclic plasticity model that can be employed in steel structural analysis. Details can be found in this repository: <https://github.com/hfx07/upm>.

**Acknowledgements.** The author acknowledges the financial support for this work from the State Key Laboratory of Subtropical Building Science (Grant No. 2020ZB22), Guangdong Basic and Applied Basic Research Foundation (Grant No. 2021A1515010610).

## References

1. Saeki E, Sugisawa M, Yamaguchi T, Wada A (1998) Mechanical properties of low yield point steels. *ASCE J Mater Civil Eng* 10(3):143–152
2. Wang JJ, Shi YJ, Wang YQ (2016) Constitutive model of low-yield point steel and its application in numerical simulation of buckling-restrained braces. *ASCE J Mater Civil Eng* 28(3):04015142
3. Xu LY, Nie X, Fan JS, Tao MX, Ding R (2016) Cyclic hardening and softening behavior of the low yield point steel BLY160: experimental response and constitutive modeling. *Int J Plast* 78:44–63
4. Wang M, Fahnestock LA, Qian FX, Yang WG (2017) Experimental cyclic behavior and constitutive modeling of low yield point steels. *Constr Build Mater* 131:696–712
5. Shi G, Gao Y, Wang X, Zhang Y (2018) Mechanical properties and constitutive models of low yield point steels. *Constr Build Mater* 175:570–587
6. He Q, Chen YY, Ke K, Yam MCH, Wang W (2019) Experiment and constitutive modeling on cyclic plasticity behavior of LYP100 under large strain range. *Constr Build Mater* 202:507–521
7. Hu FX, Shi G, Shi YJ (2018) Constitutive model for full-range elasto-plastic behavior of structural steels with yield plateau: formulation and implementation. *Eng Struct* 171:1059–1070
8. Hu FX, Shi G, Shi YJ (2016) Constitutive model for full-range elasto-plastic behavior of structural steels with yield plateau: calibration and validation. *Eng Struct* 118:210–227
9. Armstrong PJ, Frederick CO (1966) A mathematical representation of the multiaxial Bauschinger effect. CEGB Report RD/B/N731. Central Electricity Generating Board, Berkeley, UK
10. Ucak A, Tsopelas P (2011) Constitutive model for cyclic response of structural steels with yield plateau. *ASCE J Struct Eng* 137(2):195–206
11. Jia LJ, Kuwamura H (2014) Ductile fracture simulation of structural steels under monotonic tension. *ASCE J Struct Eng* 140(5):472–482